Molecular Orbital Study of the First Excited State of the OLED Material Tris(8-hydroxyquinoline)aluminum(III)

Mathew D. Halls and H. Bernhard Schlegel*

Department of Chemistry, Wayne State University, Detroit, Michigan 48202

Received February 6, 2001. Revised Manuscript Received May 16, 2001

Tris(8-hydroxyquinoline)aluminum(III), Alq3, is used in organic light-emitting diodes (OLEDs) as an electron transport material and emitting layer. The lowest singlet excited state (S_1) of Alq3 has been studied by the singles configuration interaction (CIS) method and time-dependent density functional theory (TD-DFT) using a hybrid functional, B3-LYP, and the 3-21+G** basis set. For comparison and calibration, 8-hydroxyquinoline has also been examined with these methods using the 3-21+G** and larger basis sets. The lowest singlet electronic transition ($S_0 \rightarrow S_1$) of Alq3 is primarily localized on one of the quinolate ligands. Comparison of the CIS optimized excited-state structure and the Hartree−Fock ground-state structure indicates that the geometric shift is mainly confined to the a-quinolate. Very similar changes are found for the S_1 state of 8-hydroxyquinoline, and these changes can be easily understood in terms of the nodal patterns of the highest occupied and lowest unoccupied molecular orbitals. The structural relaxation upon excitation, when expressed in terms of ground-state normal modes of vibration, corresponds to a quinolate skeletal vibrational mode at 534 cm^{-1} and serves to assign the vibronic structure observed in the low-temperature emission spectra. On the basis of the CIS-optimized structure of the excited state, TD-B3-LYP calculations predict an emission wavelength of 538 nm, which is comparable to 514 nm observed experimentally for solution phase photoluminescence. The Stokes shift calculated by TD-B3-LYP is 123 nm, in excellent agreement with the observed value of 126 nm.

Introduction

Organic light-emitting diodes (OLEDs) are currently under intense investigation for application in next generation display technologies. OLEDs are heterojunction devices in which layers of organic transport materials are usually incorporated into devices as amorphous thin solid films. These devices normally consist of at least one hole-transport layer and one electron-transport layer forming an organic/organic heterojunction. Holes from the anode and electrons from the cathode travel through the transport layers until they form a singlet exciton that relaxes giving rise to electroluminescence. The organic materials are chosen with close regard to their orbital energy levels, usually such that the electrons are confined to the electron-transport layer which, upon injection of holes, also acts as the emitting layer. Research into organic materials for use in OLEDs has mostly focused on conjugated polymers[1,2] or low molecular weight materials.[3] In 1987, Tang and VanSlyke,[4] reported the first efficient low molecular weight OLED. Their device was constructed of two active layers and used the metaloquinolate tris(8-hydroxyquinoline)aluminum (Alq3) as the electron-transport material and emitting layer. Following the initial report, metaloquinolates have become the focus of new electroluminescent materials research,[5,6] with Alq3 being the most often used.[7]

Although research into the development of OLEDs is more than 1 decade old, few studies of the fundamental molecular properties of metaloquinolates have appeared in the literature. This situation is beginning to improve. Andreoni and co-workers[8−10] carried out calculations of the geometry and electronic properties of Alq3 in neutral and charged states, as well as the bonding characteristics in metal−Alq3 complexes. The meridianal isomer (*mer*-Alq3) was found to be the preferred form of Alq3, being energetically more stable than the facial structure (*fac*-Alq3). Other studies have investigated alkali-metal doping in Alq3 to further contribute to the understanding of metal−Alq3 interactions.[11] With the assistance of quantum chemical calculations, assignments of the

* Corresponding author. E-mail: hbs@chem.wayne.edu.

(1) Burroughes, J. H.; Bradley, D. D. C.; Brown, A. R.; Marks, R. N.; Mackay, K.; Friend, R. H.; Burns, P. L.; Holmes, A. B. *Nature* **1990**, *347*, 539.
(2) Friend, R. H.; Gymer, R. W.; Holmes, A. B.; Burroughes, J. H.; Marks, R. N.; Taliani, C.; Bradley, D. D. C.; Dos Santos, D. A.; Bredas, J. L.; Logdlund, M.; Salaneck, W. R. *Nature* **1999**, *397*, 121.
(3) Mitsche, U.; Bäuerle, P. *J. Mater. Chem.* **2000**, *10*, 1471.
(4) Tang, C. W.; VanSlyke, S. A. *Appl. Phys. Lett.* **1987**, *51*, 913.
(5) Hamada, Y. *IEEE Trans. Electron Devices* **1997**, *44*, 1208.
(6) Chen, C. H.; Shi, J. *Coord. Chem. Rev.* **1998**, *171*, 161.
(7) VanSlyke, S. A.; Chen, C. H.; Tang, C. W. *Appl. Phys. Lett.* **1996**, *69*, 2160.
(8) Curioni, A.; Boero, M.; Andreoni, W. *Chem. Phys. Lett.* **1998**, *294*, 263.
(9) Curioni, A.; Andreoni, W. *J. Am. Chem. Soc.* **1999**, *121*, 8216.
(10) Curioni, A.; Andreoni, W.; Treusch, R.; Himpsel, R. F.; Haskal, E.; Seidler, P.; Kakar, S.; van Buuren, T.; Terminello, L. J. *Appl. Phys. Lett.* **1998**, *72*, 1575.
(11) Johansson, N.; Osada, T.; Stafstrom, S.; Salaneck, W. R.; Parente, V.; dos Santos, D. A.; Crispin, X.; Bredas, J. L. *J. Chem. Phys.* **1999**, *111*, 2157.

10.1021/cm010121d CCC: $20.00
Published on Web 06/30/2001

vibrational spectra of Alq3 in matrix isolation and thin solid films have also been reported.[12,13]

Given the intrinsic role that excited-state formation plays in OLED devices, the excited-state properties of Alq3 may be as significant or of greater significance than the ground-state properties of this material. Chemical reactions of the excited state may deplete emissive species from operating devices, potentially yielding products that quench luminescence, thereby reducing OLED output. Therefore, it is of considerable interest to characterize the excited states of Alq3. In experimental studies, Forrest and co-workers[14] observed a large shift between the optical absorption and the luminescence spectra of Alq3 (at least 0.4 eV measured peak to peak). This shift has been interpreted as the Franck−Condon shift resulting from large local conformational changes upon electronic excitation leading to strong exciton−vibrational coupling. The absorption and luminescence spectra of Alq3 were found, by Burrows et al.,[14] to be largely independent of the molecular environment, leading to the conclusion that the process giving rise to thin film electroluminescence is due to excitations localized on individual molecular sites.

The calculation of excited-state properties typically requires significantly more computational effort than is needed for the ground state. Thus far, only vertical electronic excitation energies of Alq3 have been computed using molecular orbital methods. Forrest and coworkers[14] have used a configuration interaction (CI) approach with the relatively inexpensive semiempirical method ZINDO[15] to compute the vertical excitations of Alq3. Stampor et al.[16] also employed the CI-ZINDO semiempirical method in their electroabsorption study of Alq3. Most recently, Martin et al.[17] employed time-dependent density functional theory (TD-DFT) to calculate the electronic transitions for Alq3.

Configuration interaction with all singly excited determinants (CIS) is an ab initio method that provides a cost-effective, semiquantitative approach for the study of excited-state properties. Analytical geometric gradients are available for CIS, allowing the efficient investigation of excited-state structures. In the present work, the CIS method is adopted to study the first singlet excited state (S_1) of Alq3. The excited-state equilibrium geometry is compared with the optimized ground-state structure. More accurate estimates of the excitation energies for Alq3 are computed using time-dependent density functional theory with a hybrid functional. Comparison of the Alq3 results with similar calculations for the isolated 8-hydroxyquinoline ligand show remarkable agreement, assisting in the interpretation of results. Decomposition of the geometry relaxation associated with the electronic excitation ($R_{CIS}-R_{HF}$) into ground-state normal mode contributions lends theoretical corroboration to recent experimental observations.

Methods

The calculations described here were carried out using the Gaussian suite of programs.[18] The structures of *mer*-Alq3 and 8-hydroxyquinoline were optimized in the first singlet excited state (S_1) using configuration interaction with all singly excited determinants[19] (CIS) in the frozen-core approximation and the split-valence 3-21+G** basis set.[20,21] For comparison with the 3-21+G** results, the S_1 excited-state structure for 8-hydroxyquinoline was also computed using the extensive Sadlej pVTZ electric property basis set.[22−24] To obtain estimates of the vertical electronic excitation energies which include some account of electron correlation, time-dependent density functional theory (TD-DFT)[25] using the hybrid B3-LYP functional was used with the 3-21+G** basis set for Alq3 and the 3-21+G** and 6-31G(d)[26,27] basis sets for 8-hydroxyquinoline. B3-LYP corresponds to the combination of Becke's three parameter exchange functional (B3)[28] with the Lee−Yang−Parr fit for the correlation functional (LYP).[29] For comparison with the excited-state structures, the equilibrium geometries of *mer*-Alq3 and 8-hydroxyquinoline were computed with the comparable ground-state method Hartree−Fock (HF). To investigate exciton−vibration coupling, harmonic vibrational frequencies and normal modes were computed for the ground state of *mer*-Alq3 (after full optimization) using gradient-corrected density functional theory, B-LYP, corresponding to Becke's gradient corrected exchange functional (B)[30] with the Lee−Yang−Parr fit for the correlation functional (LYP), using the split-valence polarized 6-31G(d) basis set. To compare with previous results for Alq3, calculations for the 8-hydroxyquinoline ligand were also carried out using the configuration interaction including single excitations from an active space of 15 occupied and 15 unoccupied molecular orbitals with the semiempirical method ZINDO.[15]

Results and Discussion

Alq3 is the most often used electron transport and emitting layer in OLEDs, giving rise to devices with a characteristic green electroluminescence. It is usually incorporated into heterojunction devices as amorphous thin solid films composed of weakly interacting monomers, through vacuum evaporation onto a hole transport

(12) Halls, M. D.; Aroca, R. *Can. J. Chem.* **1998**, *76*, 1730.
(13) Kushto, G. P.; Iizumi, Y.; Kido, J.; Kafafi, Z. H. *J. Phys. Chem. A* **2000**, *104*, 3670.
(14) Burrows, P. E.; Shen, Z.; McCarty, D. M.; Forrest, S. R.; Cronin, J. A.; Thompson, M. E. *J. Appl. Phys.* **1996**, *79*, 7991.
(15) Bacon, A. D.; Zerner, M. C. *Theor. Chim. Acta* **1979**, *53*, 21.
(16) Stampor, W.; Kalinowski, J.; Marconi, G.; Di Marco, P.; Fattori, V.; Giro, G. *Chem. Phys. Lett.* **1998**, *283*, 373.
(17) Martin, R. L.; Kress, J. D.; Campbell, I. H.; Smith, D. L. *Phys. Rev. B* **2000**, *61*, 15804.
(18) Frisch, M. J.; Trucks, G. W.; Schlegel, H. B.; Scuseria, G. E.; Robb, M. A.; Cheeseman, J. R.; Zakrzewski, V. G.; Montgomery, J. A.; Stratmann, R. E.; Burant, J. C.; Dapprich, S.; Millam, J. M.; Daniels, A. D.; Kudin, K. N.; Strain, M. C.; Farkas, O.; Tomasi, J.; Barone, V.; Cossi, M.; Cammi, R.; Mennucci, B.; Pomelli, C.; Adamo, C.; Clifford, S.; Ochterski, J.; Petersson, G. A.; Ayala, P. Y.; Cui, Q.; Morokuma, K.; Malick, D. K.; Rabuck, A. D.; Raghavachari, K.; Foresman, J. B.; Cioslowki, J.; Ortiz, J. V.; Stefanov, B. B.; Liu, G.; Liashenko, A.; Piskorz, P.; Komaromi, I.; Gomperts, R.; Martin, R. L.; Fox, D. J.; Keith, T.; Al-Laham, M. A.; Peng, C. Y.; Nanayakkara, A.; Gonzalez, C.; Challacombe, M.; Gill, P. M. W.; Johnson, B. G.; Chen, W.; Wong, M. W.; L Andres, J.; Head-Gordon, M.; Replogle, E. S.; Pople, J. A. *GAUSSIAN 98*; Gaussian, Inc.: Pittsburgh, PA, 1998.
(19) Foresman, J. B.; Head-Gordon, M.; Pople, J. A.; Frisch, M. J. *J. Phys. Chem.* **1992**, *96*, 135.
(20) Binkley, J. S.; Pople, J. A.; Hehre, W. J. *J. Am. Chem. Soc.* **1980**, *102*, 939.
(21) Gordon, M. S.; Binkley, J. S.; Pople, J. A.; Pietro, W. J.; Hehre, W. J. *J. Am. Chem. Soc.* **1983**, *104*, 2797.
(22) Sadlej, A. J. *Collect. Czech. Chem. Commun.* **1988**, *53*, 1995.
(23) Sadlej, A. J. *Theor. Chim. Acta* **1992**, *79*, 123.
(24) Sadlej's polarized electric property basis set was obtained from the Extensible Computational Chemistry Environment Basis Set Database, Version 1.0, Pacific Northwest Laboratory, P.O. Box 999, Richland, WA 99352 (http://www.emsl.pnl.gov: 2080/forms/basisform-.html).
(25) Stratmann, R. E.; Scuseria, G. E.; Frisch, M. J. *J. Chem. Phys.* **1998**, *109*, 8218.
(26) Hehre, W. J.; Ditchfield, R.; Pople, J. A. *J. Chem. Phys.* **1972**, *56*, 2257.
(27) Francl, M. M.; Petro, W. J.; Hehre, W. J.; Binkley, J. S.; Gordon, M. S.; DeFrees, D. J.; Pople, J. A. *J. Chem. Phys.* **1982**, *77*, 3654.
(28) Becke, A. D. *J. Chem. Phys.* **1993**, *98*, 5648.
(29) Lee, C.; Yang, W.; Parr, R. G. *Phys. Rev. B* **1988**, *37*, 785.
(30) Becke, A. D. *Phys. Rev. A* **1988**, *38*, 3098.

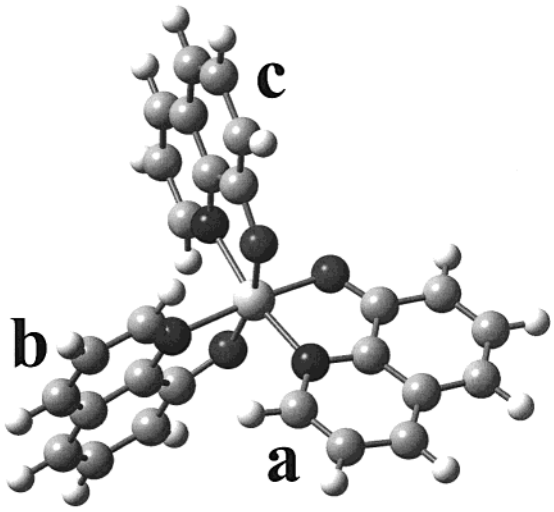

Figure 1. Structure of the meridianal geometric isomer of Alq3 (*mer*-Alq3) with labels a−c designating the three quinolate ligands.

layer (typically an aromatic amine) on a supporting anode substrate. A cathode layer is then deposited over the Alq3 film. Experimental studies of the absorption and luminescence spectra of metaloquinolates (Mq3; M = Al, Ga, In) in solution and in thin solid films indicate that the low-energy excited states of these materials are localized on individual molecular sites.[14] Therefore, valuable insight may be obtained from molecular calculations.

The majority of the work carried out thus far has been on the ground-state characteristics of Alq3. Alq3 has two geometric isomers, the facial (*fac*-Alq3) and meridianal (*mer*-Alq3) forms having C_3 and C_1 symmetries, respectively. Both experimental and theoretical studies indicate that *mer*-Alq3 is the dominant form. Sheppard and co-workers[31] performed an analysis of the proton NMR spectra of Alq3 and were unable to detect resonances from *fac*-Alq3. Kafafi and co-workers[13] carried out a low-temperature matrix isolation infrared study of Alq3 and found little or no evidence for the presence of the facial isomer. Curioni et al.[8] carried out calculations using the gradient-corrected density functional, B-LYP, and a plane wave-pseudopotential basis on both geometric isomers of Alq3 and found that *mer*-Alq3 was ca. 4 kcal mol^{-1} lower in energy than the facial isomer. In the work by Kafafi and co-workers,[13] quantum chemical calculations were performed to assist in the interpretation of the infrared spectra of Alq3. Their results using the hybrid density functional, B3-LYP, and the SDD basis set puts *mer*-Alq3 ca. 8 kcal mol^{-1} lower in energy then *fac*-Alq3. Therefore, the calculations presented here will consider *mer*-Alq3 exclusively.

Ground-State Geometry and Electronic Structure. *Ground-State Geometry.* The structure of *mer*-Alq3 is shown in Figure 1, with labels a−c designating the three different quinolate ligands. The structure is such that the central Al atom (+3 formal oxidation state) is surrounded by the three quinolate ligands in a pseudooctahedral configuration with the a- and c-quinolate nitrogens and the b- and c-quinolate oxygens trans to each other. In the current study, the ground-state geometry of *mer*-Alq3 was computed at the HF/3-21+G** level of theory to enable comparison with the excited-state structure computed with the CIS/3-21+G** method. The ground-state structure of Alq3 has been studied extensively by a number of groups,[8−11,13] and the results of the present calculations are in excellent agreement with previous determinations. The bond distances of the inner coordination sphere are given in Table 1, along with data from previous theoretical studies and from experimental determinations.[32,33] An immediate observation is the structural parameters obtained using the semiempirical methods AM1 and PM3 are in poor agreement with experiment and the first-principle methods, tending to severely overestimate and underestimate the Al−N and the Al−O, respectively. This fact has been attributed previously to inadequate parametrization,[8] as is suggested by noting that the ZINDO distances show significantly better agreement. The overall agreement for each level of theory can be evaluated through comparison with the average of the experimental determinations. Comparison with the experimental data indicates that the Hartree−Fock/3-21+G** structural parameters are in similar or better agreement than the density functional methods. It is well-known that the reliability of predicted molecular geometries is heavily dependent on the quality of basis set employed, with electron correlation having less of an effect. The agreement in Table 1 suggests that the level of representation of the valence region using the 3-21+G** basis set is sufficient to describe the ligand−Al interactions and the overall structure of *mer*-Alq3.

Orbital Shapes. A number of theoretical studies of the electronic structure of Alq3 have been reported,[10,11,34−37] which complement the extensive experimental studies that have been carried out using optical and ultraviolet photoelectron spectroscopies.[36−40] The interpretation of observed spectral features is greatly assisted by molecular orbital calculations, which, in addition to providing orbital energies for comparison with experiment, furnish a detailed description of orbitals, including spatial characteristics, nodal patterns, and individual atom contributions. The frontier orbital levels of Alq3 consist of sets of closely spaced "triplets". The highest occupied molecular orbitals (HOMOs) and the lowest unoccupied molecular orbitals (LUMOs) of Alq3 largely preserve the electronic structure of the individual 8-hydroxyquinoline ligands with little contribution from the central aluminum. The first in-depth report of the electronic structure

(31) Addy, P.; Evans, D. F.; Sheppard, R. N. *Inorg. Chim. Acta* **1987**, *127*, L19.

(32) Fujii, I.; Hirayama, N.; Ohtani, J.; Kodama, K. *Anal. Sci.* **1996**, *12*, 153.

(33) Schmidbaur, H.; Lettenbaur, J.; Wilkinson, D. L.; Müller, G.; Kumberger, O. *Z. Naturforsch. B* **1991**, *46*, 901.

(34) Zhang, R. Q.; Lee, C. S.; Lee, S. T. *J. Chem. Phys.* **2000**, *112*, 8614.

(35) Zhang, R. Q.; Lee, C. S.; Lee, S. T. *Chem. Phys. Lett.* **2000**, *326*, 413.

(36) Sugiyama, K.; Yoshimura, D.; Miyamae, T.; Ishii, H.; Ouchi, Y.; Seki, K. *J. Appl. Phys.* **1998**, *83*, 4928.

(37) Hill, I. G.; Kahn, A.; Cornil, J.; dos Santos, D. A.; Brédas, J. L. *Chem. Phys. Lett.* **2000**, *317*, 444.

(38) Schmidt, A.; Anderson, M. L.; Armstrong, N. R. *J. Appl. Phys.* **1994**, *78*, 5619.

(39) Rajagopal, A.; Wu, C. I.; Kahn, A. *J. Appl. Phys.* **1998**, *83*, 2649.

(40) Hopkins, T. A.; Meerholz, K.; Shaheen, S.; Anderson, M. L.; Schmidt, A.; Kippelen, B.; Padias, A. B.; Halls, H. K.; Peyghambarian, N.; Armstrong, N. R. *Chem. Mater.* **1996**, *8*, 344.

Table 1. HF/3-21+G Ground-State and CIS/3-21+G** Excited-State Al−N and Al−O Bond Lengths (Å) for *mer*-Alq3 along with Those from Previous Theoretical Ground-State Investigations and X-ray Analysis for Comparison**

	S_0												S_1	
bond	HF/ 3-21+G **	B3L YP/ SDD[a]	B3LY P/ 6-31G(d) [b]	BLYP/ DNP[c]	BLY P/ PW-PP[a]	AM1[d]	PM3 [d]	ZIND O[e]	X-ray[f]	X-ray[g]	X-ray [h]	Exp Avg	CIS/ 3-21+G **	% diff[i]
Al−N_a	2.063	2.084	2.08	2.019	2.089	2.38	2.30	2.08	2.035	2.048	2.050	2.044	1.982	−3.94
Al−N_b	2.033	2.056	2.06	2.019	2.073	2.40	2.33	2.08	2.033	2.026	2.017	2.025	2.061	1.37
Al−N_c	2.117	2.114	2.13	2.051	2.151	2.49	2.43	2.13	2.078	2.073	2.087	2.079	2.065	−2.46
Al−O_a	1.826	1.885	1.86	1.839	1.860	1.77	1.80		1.849	1.841	1.850	1.847	1.909	4.58
Al−O_b	1.866	1.918	1.89	1.868	1.885	1.77	1.79		1.858	1.882	1.860	1.867	1.859	−0.36
Al−O_c	1.856	1.915	1.88	1.864	1.880	1.76	1.78		1.863	1.849	1.857	1.856	1.861	0.25

[a] Kushto et al. (2000).[13] [b] Martin et al. (2000).[17] [c] Johansson et al. (1999).[11] [d] Curioni et al. (1998).[8] [e] Burrows et al. (1996).[14] [f] Fujii et al. (1996).[32] [g] Schmidbaur et al. (1991).[33] [h] Brinkmann et al. (2000).[45] [i] % difference defined as $((R_{CIS} - R_{HF})/R_{HF}) \times 100\%$.

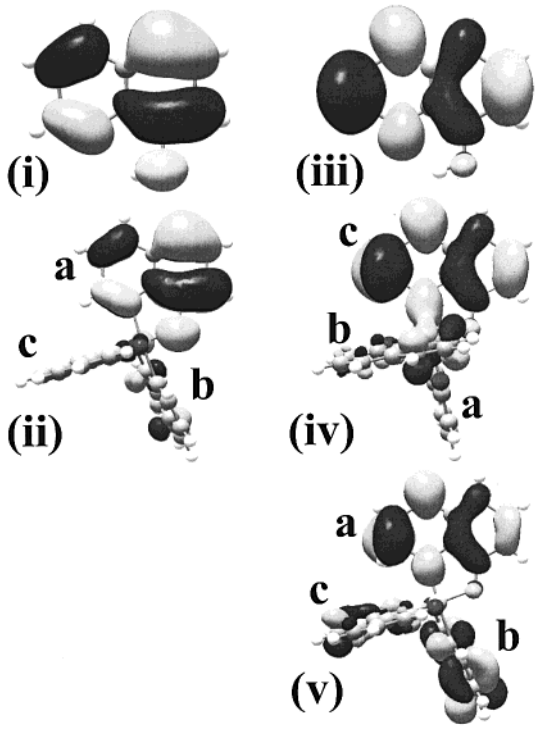

Figure 2. Molecular orbital surfaces of the (i) HOMO of 8-hydroxyquinoline, (ii) least bound HOMO of *mer*-Alq3, (iii) LUMO of 8-hydroxyquinoline, (iv) lowest energy LUMO of *mer*-Alq3 and (v) second lowest energy LUMO of *mer*-Alq3. (0.02 e au^{-3}).

of Alq3 was provided by Curioni et al.[8] Using gradient-corrected DFT, they compared the electronic structure of the two isomers of Alq3 and observed that the molecular orbitals of *mer*-Alq3 were more strongly localized than in *fac*-Alq3. They found that the three HOMO orbitals of *mer*-Alq3 are split in energy and the least bound orbital in the HOMO triplet is mainly localized on one ligand, whereas the other orbitals are predominantly on the other ligands. The HOMO for 8-hydroxyquinoline and the least bound HOMO orbital for *mer*-Alq3 computed using HF/3-21+G** are shown in Figure 2 (i and ii, respectively). In agreement with the previous DFT study the highest HOMO level is mainly localized on a single ligand, the a-quinolate ligand depicted in Figure 1. The LUMO orbital for 8-hydroxyquinoline and the lowest and second lowest energy LUMO orbitals for *mer*-Alq3 are also shown in Figure 2 (iii−v, respectively). The correlation between the free ligand orbitals and *mer*-Alq3 orbitals is clear. The results presented here are consistent with previous theoretical studies with the HOMO and LUMO orbitals strongly localized on the phenoxide side and pyridyl side of the ligands, respectively. This localization is more evident if the molecular orbitals shown in Figure 2 are plotted with smaller isosurface values. The ground-state dipole moment of *mer*-Alq3 is predicted to be 5.51 D at the HF/3-21+G** level of theory. This value compares well with the calculated result of Martin et al.[17] of 5.3 D, using hybrid DFT (B3-LYP) and the 6-31G(d) basis set.

Orbital Energies. The energies of the HOMO triplet for *mer*-Alq3 computed at the HF/3-21+G** level of theory are −7.47, −7.73, and −7.88 eV. The HOMO energies agree with the energy splitting predicted by the DFT results, with the highest level split ca. 0.3 eV from the next occupied level which is only split by about half this amount (ca. 0.15 eV) from the last level in the HOMO triplet. The numerical value for the HOMO energy computed at the HF/3-21+G** level of theory is in good agreement with reported experimental determinations. Recently the gas-phase ionization energy of Alq3 has been reported to be 7.25 eV.[41] Within Koopman's approximation[42] this value can be compared to the computed binding energy of the least bound electronic level (HOMO). The computed energy of the HOMO agrees favorably with the experimental gas-phase ionization energy of Alq3, agreeing within ca. 0.2 eV. Experimental determinations of the ionization energy for Alq3 in thin solid films typically report values in the range from 6.4 [43] to 6.65 eV.[38,40] The condensed phase polarization energy, estimated by comparison of experimental gas-phase ionization energy and thin film values, gives a value of ca. 0.7 eV. This value is in the typical range of the polarization energies reported for organic solids.[44]

$S_0 \rightarrow S_1$ Excitation Energy and the S_1 Excited-State Structure. Experimental investigations of the excited-state properties of Alq3 have studied the photoabsorption, photoluminescence, and electroluminescence of this key OLED material.[13,14,17,38,40,45−48,50] Inspection of the absorption and emission spectra from metaloquinolates (Mq3; M = Al, Ga, In, Sc) in solvated and condensed-phase systems shows that the spectra are largely independent of the molecular environment and the emissive states are localized on individual molecular sites.[14,46] Comparison of the spectra from

(41) Slattery, D. K.; Linkous, C. A.; Gruhn, N. *Polym. Prepr.* **2000**, *41*, 866.
(42) Szabo, A.; Ostlund, N. S. *Modern Quantum Chemistry*; Dover Publication Inc.: New York, 1996; p 127.
(43) Hill, I. G.; Kahn, A.; Soos, Z. G.; Pascal, R. A. *Chem. Phys. Lett.* **2000**, *327*, 181.
(44) Sato, N.; Seiki, K.; Inokuchi, J. *J. Chem. Soc., Faraday Trans.* **1981**, *277*, 1621.

metaloquinolates with different metal centers and with the spectra from 8-hydroxyquinoline further suggests that the excited states involved in the luminescence are ligand localized.[14,47] Previous theoretical investigations and the results presented here support the localized nature of the orbitals involved in the lowest energy electronic transitions in Alq3. The lowest electronic transitions are $\pi \rightarrow \pi^*$ transitions in the quinolate rings, involving partial charge transfer from the phenoxide side to the pyridyl side. The experimental absorption spectrum of vacuum deposited Alq3 thin films shows two maxima at ca. 385 and 260 nm (3.22 and 4.77 eV, respectively).[48] These electronic excitations can be unambiguously assigned to the lower energy ^1L_a and the higher energy ^1B_b excited states of 8-hydroxyquinoline.[49,50] Solution phase investigations observe an absorption maximum at ca. 390 nm (3.18 eV), in close agreement with the thin film measurement.[40]

The vertical electronic excitations for Alq3 have been computed previously by a number of investigators. Burrows et al.[14] used the ZINDO semiempirical method with configuration interaction (CI) including all single configurations from the highest 15 occupied and lowest 15 virtual orbitals to compute the lowest excited states for Alq3. They obtained a lowest electronic transition of 377 nm (3.28 eV), which compares favorably with the experimental value of ca. 385−390 nm (3.22−3.18 eV). Stampor et al.[16] also used a CI-ZINDO approach with 144 singly excited configurations to compute the vertical excitation energies for Alq3 which gave a lowest energy singlet transition of 356 nm (3.48 eV). The most sophisticated calculation of the excitation energies for Alq3 has used time-dependent density functional theory (TD-DFT) with the hybrid B3-LYP functional and the medium-sized polarized split-valence 6-31G(d) basis set.[17] The lowest energy singlet transition having significant oscillator strength computed with TD-B3-LYP/6-31G(d) was at 427 nm (2.90 eV), deviating from the experimental data by ca. 42−37 nm (0.3−0.28 eV). Better agreement using TD-DFT may be attainable using a basis set with extra representation in the valence region, particularly having additional augmentation with diffuse functions.

$S_0 \rightarrow S_1$ Vertical Excitation Energy. In the present study, configuration interaction with all singly (CIS) excited determinants is employed to study the lowest energy singlet excited state (S_1) of Alq3. CIS represents for excited states a general zeroth-order method, just as Hartree−Fock is for the ground state of molecular systems. Besides being relatively inexpensive, permitting it to be applied to large molecules such as Alq3, analytic derivatives are available for CIS allowing the efficient calculation of excited-state structures and properties.[19,51] The vertical excitation energies computed using CIS and the 3-21+G** basis set for both the free 8-hydroxyquinoline ligand and *mer*-Alq3 are presented in Table 2. Comparison of the CIS/3-21+G** vertical excitation energies for free 8-hydroxyquinoline ligand and *mer*-Alq3 with the experimental values shows that the CIS calculations clearly overestimate the lowest excitation energies by ca. 1.5 eV. CIS theory is known to overestimate electronic excitation energies, due to the neglect of the effects of electron correlation and higher order excitations. To investigate the effect of electron correlation on the computed energies, calculations using time-dependent density functional theory and the hybrid density functional, B3-LYP, were carried out with the 3-21+G** basis set for the free ligand and *mer*-Alq3, so direct comparison with the CIS/3-21+G** results can be made. For *mer*-Alq3 the TD-DFT calculations were carried out at the HF/3-21+G**-optimized structure. To complement the previous study on Alq3 by Martin et al.,[17] time-dependent B3-LYP calculations using the 6-31G(d) basis set were also performed for 8-hydroxyquinoline. Recent work by Stratmann et al.[25] has shown that time-dependent density functional theory yields significantly better results than those provided by Hartree−Fock-based methods such as the random-phase approximation (RPA) or CIS yet is similar in cost. Due to the description of the orbitals involved in the transition and the computed oscillator strength, the second singlet transition computed using TD-B3-LYP for *mer*-Alq3 is compared to the CIS results presented here. Comparison of the TD-B3-LYP excitation energies in Table 2 with the experimental values shows improved agreement over the CIS results. Additional CIS calculations for 8-hydroxyquinoline were performed using the extensive Sadlej pVTZ electric property basis set. These results are also shown in Table 2. A surprising result is that the CIS/Sadlej pVTZ excitation energy computed for 8-hydroxyquinoline is in worse agreement with the experimental value than the CIS calculations with the smaller basis set. Pople and co-workers[19] observed that with the CIS method, the use of basis sets that included significant polarization resulted in a larger overestimation of excitation energies; however, the excited-state potential energy surface was found to be more accurate. This behavior was attributed to the fact that these functions lower the ground-state reference energies to

Table 2. CIS/3-21+G S_0 to S_1 Vertical Electronic Transition Wavelengths (nm) and Energies (in Parentheses (eV)) for 8-Hydroxyquinoline (8Hq) and *mer*-Alq3 along with Data from Previous Theoretical Studies and Experiments for Comparison**

	8Hq	*mer*-Alq3
CIS/3-21+G**	232 (5.35)	265 (4.68)
CIS/Sadlej pVTZ	214 (5.80)	
TD-B3-LYP/6-31G(d)	333 (3.72)	427 (2.90)[a,b]
TD-B3LYP/3-21+G**	330 (3.76)	415 (3.0)[b,c]
CI-ZINDO	324 (3.83)	356 (3.48),[d] 377 (3.28)[e]
expt	323 (3.84)[f]	390 (3.18),[g] 385 (3.22)[h]

[a] Martin et al. (2000).[17] [b] Based on oscillator strength and orbital descriptions; the second singlet transition computed using TD-DFT is listed for comparison (see ref 17). [c] TD-B3-LYP/3-21+G** excitation energy computed at the HF/3-21+G** optimized structure for *mer*-Alq3. [d] Stampor et al. (1998).[16] [e] Burrows et al. (1996).[14] [f] Perkampus et al. (1962).[50] [g] Hopkins et al. (1996).[40] [h] Garbuzov et al. (1996).[48]

(45) Brinkmann, M.; Gadret, G.; Muccini, M.; Taliani, C.; Masciocchi, N.; Sironi, A. *J. Am. Chem. Soc.* **2000**, *122*, 5147.
(46) Burrows, P. E.; Sapochak, L. S.; McCarty, D. M.; Forrest, S. R.; Thompson, M. E. *Appl. Phys. Lett.* **1994**, *64*, 2718.
(47) Humbs, W.; van Veldhoven, E.; Zhang, H.; Glasbeek, M. *Chem. Phys. Lett.* **1999**, *304*, 10.
(48) Garbuzov, D. Z.; Bulovic, V.; Burrows, P. E.; Forrest, S. R. *Chem. Phys. Lett.* **1996**, *249*, 533.
(49) Klevens, H. B.; Platt, J. R. *J. Chem. Phys.* **1949**, *17*, 470.
(50) Perkampus, H. H.; Kortüm, K. *Z. Anal. Chem.* **1962**, *190*, 111.
(51) Foresman, J. B.; Schlegel, H. B. In *Recent experimental and computational advances in molecular spectroscopy*; Gausto, R., Hollas, J. M., Eds.; Kluwer Academic: Dordrecht, The Netherlands, 1993; Vol. 406, p 11.

Table 3. HF/3-21+G Ground-State and CIS/3-21+G** Excited-State Bond Lengths for the a-, b-, and c-Quinolate Ligands in *mer*-Alq3 and for 8-Hydroxyquinoline (8Hq), along with HF/Sadlej PVTZ Ground-State and CIS/Sadlej PVTZ Excited-State Bond Lengths for 8Hq for Comparison**

	HF/Sadlej	HF/3-21+G**				CIS/Sadlej	CIS/3-21+G**				HF/Sadlej	HF/3-21+G** % diff[a]			
	8Hq	8Hq	a-Alq3	b-Alq3	c-Alq3	8Hq	8Hq	a-Alq3	b-Alq3	c-Alq3	% diff[a] 8Hq	8Hq	a-Alq3	b-Alq3	c-Alq3
C_3–N_4	1.292	1.306	1.309	1.309	1.311	1.359	1.379	1.385	1.309	1.311	5.20	5.64	5.78	0.05	0.02
C_{10}–C_9	1.361	1.357	1.368	1.367	1.368	1.423	1.418	1.434	1.367	1.368	4.59	4.47	4.80	−0.01	−0.01
C_7–C_8	1.360	1.365	1.368	1.36 8	1.369	1.424	1.430	1.421	1.368	1.369	4.77	4.77	3.87	0.02	−0.02
C_2–C_1	1.358	1.362	1.366	1.36 7	1.368	1.416	1.420	1.417	1.367	1.368	4.23	4.24	3.75	0.01	0.01
C_6–C_5	1.402	1.401	1.395	1.39 2	1.393	1.429	1.427	1.402	1.392	1.393	1.95	1.88	0.45	0.00	−0.04
C_5–C_{10}	1.427	1.416	1.424	1.42 3	1.421	1.425	1.414	1.429	1.421	1.422	−0.10	−0.09	0.37	−0.11	0.05
C_1–C_6	1.417	1.420	1.417	1.41 9	1.419	1.398	1.404	1.411	1.419	1.419	−1.32	−1.12	−0.44	−0.02	−0.01
C_6–C_7	1.419	1.418	1.419	1.42 0	1.419	1.402	1.402	1.409	1.420	1.419	−1.18	−1.09	−0.64	0.01	0.00
N_4–C_5	1.352	1.362	1.365	1.36 0	1.360	1.319	1.331	1.348	1.360	1.361	−2.45	−2.27	−1.25	−0.04	0.06
C_2–C_3	1.417	1.418	1.412	1.41 4	1.415	1.369	1.371	1.367	1.414	1.414	−3.39	−3.34	−3.19	0.01	−0.08
C_{10}–O_{11}	1.338	1.378	1.336	1.34 3	1.338	1.308	1.347	1.288	1.343	1.340	−2.19	−2.24	−3.61	−0.04	0.16
C_8–C_9	1.416	1.416	1.416	1.41 9	1.418	1.363	1.366	1.365	1.419	1.418	−3.73	−3.52	−3.61	0.01	0.00
C_2–H_{13}	1.079	1.069	1.069	1.06 9	1.069	1.079	1.069	1.070	1.069	1.069	0.00	0.01	0.07	0.00	−0.02
C_7–H_{15}	1.079	1.071	1.070	1.07 0	1.070	1.080	1.071	1.070	1.071	1.070	0.06	0.00	−0.03	0.01	0.00
C_9–H_{17}	1.078	1.069	1.069	1.069	1.069	1.077	1.068	1.068	1.069	1.069	−0.10	−0.07	−0.07	−0.01	0.00
C_3–H_{14}	1.082	1.069	1.067	1.068	1.068	1.079	1.067	1.066	1.068	1.069	−0.25	−0.20	−0.14	−0.04	0.03
C_8–H_{16}	1.080	1.070	1.071	1.07 1	1.071	1.079	1.069	1.069	1.071	1.071	−0.14	−0.13	−0.15	0.00	0.00
C_1–H_{12}	1.080	1.071	1.071	1.07 2	1.072	1.078	1.070	1.069	1.072	1.071	−0.16	−0.13	−0.23	0.00	−0.01
O_{11}–X_{18}	0.949	0.947	1.826	1.86 6	1.856	0.957	0.953	1.909	1.859	1.861	0.78	0.71	4.58	−0.36	0.25
N_4–Al			2.063	2.03 3	2.117			1.982	2.061	2.065			−3.94	1.37	−2.46

[a] % difference defined as $((R_{CIS} - R_{HF}) \times 100\%$.

a greater extent than the excited-state energies. Finally, for completeness sake, calculations using a configuration interaction (CI) approach over an active space of 15 occupied and 15 unoccupied molecular orbitals with the semiempirical ZINDO method (as in ref 14) was carried out on 8-hydroxyquinoline to complement similar calculations previously carried out for *mer*-Alq3. The CI-ZINDO results, shown in Table 2, demonstrate the capability of semiempirical methods to compute molecular properties for which they were specifically parametrized.

S_1 Excited-State Structure. Studies of the excited-state properties for a number of molecules using the CIS method have found that despite the tendency of CIS to overestimate electronic transition energies, the excited-state potential energy surface can often be quite accurate, as evidenced by comparison of equilibrium excited-state structures and vibrational frequencies with experiment.[19] Experimental studies of Alq3 have observed a large shift (0.4−0.7 eV) between the optical absorption spectra and emission spectra, thought to arise from significant differences between the ground-state and excited-state structures. To investigate the geometry change associated with electronic excitation to the lowest energy singlet excited state ($S_0 \rightarrow S_1$), the geometry of *mer*-Alq3 was optimized at the CIS/3-21+G** level of theory in the S_1 state for comparison with the HF/3-21+G** ground-state structure. Similar calculations were carried out for 8-hydroxyquinoline for comparison. Table 3 presents the optimized ground- and excited-state bond lengths for 8-hydroxyquinoline and *mer*-Alq3. Note that positive and negative values in the % difference columns indicate bond elongation and contraction in the excited state, respectively. Figure 3 shows the structure of the 8-hydroxyquinoline ligand and the atom labels used in Table 3. Comparison of the excited- and ground-state geometries for a-, b-, and c-quinolates in *mer*-Alq3 indicates that the structural shift is predominantly localized on the a-quinolate. The b- and c-quinolates in *mer*-Alq3 are practically unaffected except for changes in the Al−O and Al−N bond lengths. The CIS/3-21+G** excited-state relaxation

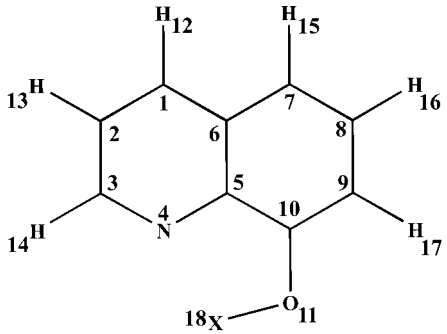

Figure 3. Structure and atom labels of the quinolate ligand used to discuss the structural shift upon electronic excitation ($S_0 \rightarrow S_1$) in text and Table 3.

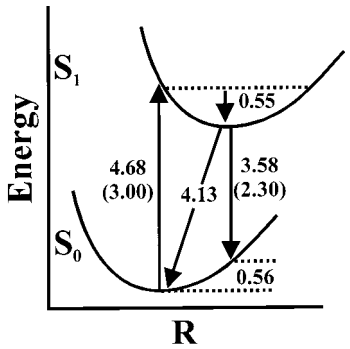

Figure 4. Diagram summarizing the CIS/3-21+G** transition and relaxation energies (in eV) for *mer*-Alq3. Parenthetical values correspond to TD-B3-LYP/3-21+G** results for comparison.

energy is calculated to be 0.55 eV as indicated in Figure 4. The excited-state dipole moment for *mer*-Alq3 is predicted to be 2.99 D, which is ca. 2.5 D less than the predicted ground-state dipole moment. Comparing the structural shift between the excited and ground state for the a-quinolate and 8-hydroxyquinoline shows a remarkable similarity. Hartree−Fock and CIS geometry optimizations were carried out for 8-hydroxyquinoline using the Sadlej pVTZ basis set to ensure the basis set consistency of the results presented here. The data presented in Table 3 shows that the excited-state

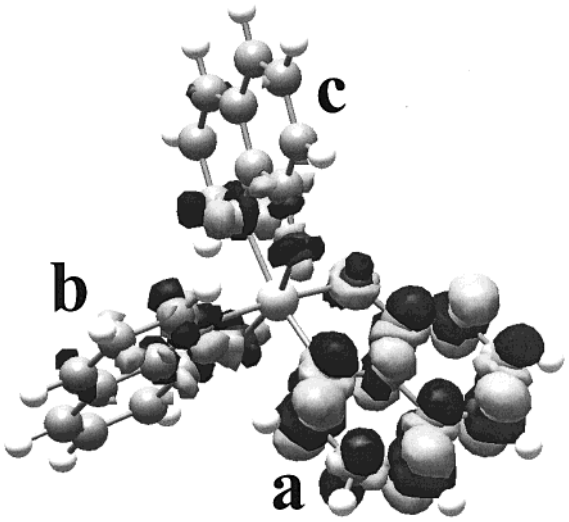

Figure 5. Electron density difference between the CIS/3-21+G** S_1 excited state and the HF/3-21+G** ground state for *mer*-Alq3. (2×10^{-6} e au^{-3}).

geometry change predicted with the 3-21+G** and the Sadlej pVTZ basis sets are in excellent agreement.

Orbital Analysis. The lowest energy singlet transition for *mer*-Alq3 at the CIS/3-21+G** level of theory involves transitions from the least bound HOMO orbital (ii in Figure 2) to the lowest and the second lowest energy LUMO orbitals (iv and v in Figure 2) with equal weight. The least bound HOMO orbital of *mer*-Alq3 is mainly localized on the a-quinolate, but the LUMOs also have contributions from the other rings. The site of the electronic excitation can be readily identified by considering the difference in total electron density between the excited and ground states. The total electron density difference between the excited state and the ground state is shown in Figure 5. The localized nature of the electronic excitation is clear, with only the a-quinolate having significant amplitude.

The observed geometry relaxation in 8-hydroxyquinoline and *mer*-Alq3 can be rationalized by consideration of the nodal patterns of the HOMO and LUMO orbitals in Figure 2. The lowest energy singlet excitation ($S_0 \rightarrow S_1$) is mainly HOMO $\rightarrow$ LUMO in character. The LUMO has nodes across the C_2–C_1, C_3–N_4, C_7–C_8, and C_{10}–C_9 bonds, but the HOMO is bonding in these regions. Therefore one would expect elongation of these bonds; Table 3 shows that these bonds are in fact considerably longer in the excited state. The HOMO has a node across the C_2–C_3 and C_8–C_9 bonds while the LUMO is bonding. The data in Table 3 confirms the anticipated contraction of these bonds.

$S_1 \rightarrow S_0$ Emission Energy. From the difference between the HF/3-21+G** ground-state energy and the CIS/3-21+G** excited-state energy, the adiabatic excitation energy is estimated to be ca. 4.13 eV (without ZPE corrections) as indicated in Figure 4. The CIS calculations for *mer*-Alq3 also provide an estimate of the relaxed emission energy from the optimized CIS excited-state structure to the Hartree−Fock ground state ($S_1 \rightarrow S_0$). The emission is calculated to be ca. 347 nm (3.58 eV), which, as with the predicted absorption energies, severely overestimates the energy of the experimental photoluminescence emission observed in solution at ca. 514 nm (2.41 eV)[40] and the electroluminescence emission observed in devices at ca. 519 nm (2.39 eV).[5] The difference between the calculated absorption and emission wavelengths, ca. 82 nm, can be compared to the experimental Stokes shift for Alq3 in solution which is reported at 126 nm.[40] TD-B3-LYP/3-21+G** calculations were carried out for *mer*-Alq3 at the CIS/3-21+G**-optimized excited-state structure to obtain more accurate estimates of the emission energy. With TD-B3-LYP, the emission energy is predicted to be ca. 2.30 eV corresponding to emission at ca. 538 nm, which is in much closer agreement with the experimental observations. The estimated Stokes shift at the TD-B3-LYP/3-21+G** level of theory is ca. 123 nm, which is in good agreement with the experimental value, lending support for the excited-state geometry shift described here. The calculated estimates for the absorption and emission energies, computed at the CIS/3-21+G** and TD-B3-LYP/3-21+G** levels of theory, for *mer*-Alq3 are summarized in Figure 4.

S_0−S_1 Vibrational Coupling. Recently, experimental investigations of the vibronic coupling between the ground state (S_0) and first excited singlet state (S_1) of Alq3 have been reported. Masciocchi and co-workers[45] studied the low-temperature (4.2 K) fluorescence spectrum of Alq3 from single crystal and polycrystalline samples and observed vibronic structure with a ca. 525 cm^{-1} spacing. It was concluded that the vibrational coupling was mainly due to one intramolecular mode, independent of the crystal structure. The mode was assigned, by comparison to related molecules, to an in-plane bending mode observed at ca. 526 cm^{-1} in the Raman spectrum of Alq3. However, coupling contributions from other vibrational modes could not be ruled out. Kafafi and co-workers[13] studied the low-temperature (11 K) matrix-isolated photoluminescence spectrum of Alq3. Vibronic structure was observed on the emission band with an energy spacing of ca. 700 cm^{-1}. An asymmetric combination of ring-breathing and Al-ligand stretching mode, observed in the infrared spectra at ca. 652 cm^{-1}, was assigned to be the most likely coupling vibration.

To investigate the vibrational coupling between the ground and first excited state of Alq3, the structural shift for *mer*-Alq3, defined as the difference between the excited state and ground-state geometries ($R_{\mathrm{CIS/3-21+G^{**}}} - R_{\mathrm{HF/3-21+G^{**}}}$), was decomposed into a linear combination of ground-state normal modes.[52] To obtain more accurate normal coordinates to perform the decomposition over, the gradient-corrected density functional B-LYP was used with the 6-31G(d) basis set to compute analytical harmonic frequencies, normal modes, and infrared intensities.[53] The B-LYP/6-31G(d) infrared spectrum for *mer*-Alq3 and the experimental spectrum are shown in Figure 6. The agreement between the experiment and the theoretical spectrum is excellent, lending support for the force constants and normal coordinates provided by the B-LYP/6-31G(d) calculations. Table 4 presents the theoretical frequencies,

(52) Linear decomposition of the difference between ground and first excited-state geometries was carried out using *Mathematica*, following a least-squares structural alignment of the HF- and CIS-optimized structures to minimize the contributions from rotational degrees of freedom: Wolfram, S. *Mathematica*, 3rd ed.; Cambridge University Press: Cambridge, U.K., 1996. And see associated computer programs, Wolfram Research, Inc., Champaign, IL.

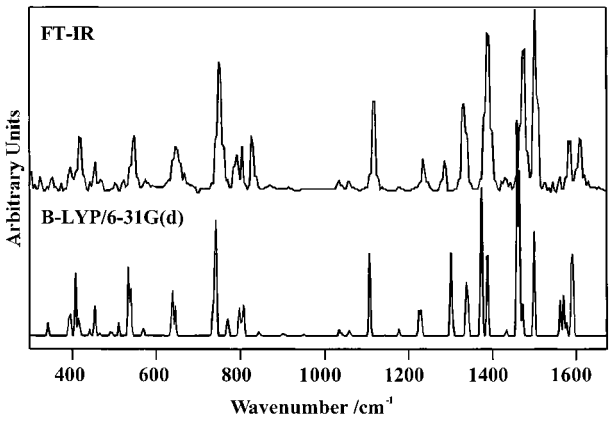

Figure 6. B-LYP/6-31G(d) infrared spectrum along with the experimental infrared spectrum for *mer*-Alq3 for comparison. (Experimental infrared spectrum is from ref 12.)

Table 4. B-LYP/6-31G(d) Vibrational Frequencies, Infrared Intensities, R_{CIS}–R_{HF} Decomposition Coefficients (See Text) and Normal Mode Descriptions for the Ten Normal Modes with the Most Significant R_{CIS}–R_{HF} Decomposition Coefficients[a]

mode	B-LYP/6-31G(d) freq (cm^{-1})	I_{IR} (km mol^{-1})	coeff	mode description[b]
4	43	1.52	0.20	Al−O, Al−N def
6	49	0.50	0.15	Al−O, Al−N def
3	41	1.52	0.14	Al−O, Al−N def
5	46	0.83	0.12	Al−O, Al−N def
8	136	0.18	0.11	CCCC tors./butterfly
38	**534**	**122.80**	**0.10**	**Al−O str/CCC def**
12	180	1.88	0.08	CCCC tors/butterfly
22	343	22.73	0.08	Al−N str/CCC def
49	**637**	**45.55**	**0.07**	**Al−O, Al−N str/CCC def**
9	148	0.49	0.07	CCCC tors/butterfly

[a] Bold rows correspond to skeletal vibrations observed experimentally in the vibronic structure of the emission bands of Alq3. [b] Mode descriptions from Halls et al. (1998),[12] Kushto et al. (2000),[13] and from visualization of the B-LYP/6-31G(d) normal mode Cartesian displacement vectors.

infrared intensities, mode descriptions, and R_{CIS}-R_{HF} decomposition coefficients for the 10 normal modes with the most significant coefficients. The modes can be separated on the basis of the nature of the vibration. Typically very low-frequency modes (less than ca. 300 cm^{-1}) correspond to torsional modes. With an increase in energy the modes become more localized, corresponding to skeletal vibrations of the quinolate ligands. Consideration of the decomposition coefficients presented in Table 4 shows that the geometry change between the first excited and ground electronic states of *mer*-Alq3 has a large degree of torsional character involving motions of entire quinolate ligands with respect to each other. This is consistent with the changes in the Al−N and Al−O bond lengths, noted previously. Two skeletal vibrations appear in the list of normal modes with significant decomposition coefficients. They have predicted frequencies of 534 and 637 cm^{-1}, agreeing with the experimental observations. The decomposition coefficients separate the normal modes into two groups, normal modes with relatively large contributions (greater than or equal to 0.1) and those with weaker contributions (less than 0.1). Of the two experimentally proposed coupling vibrations, only the skeletal vibration of 534 cm^{-1} appears in the first group with a coefficient of 0.1. The normal mode displacement vectors for the vibrations at 534 and 637 cm^{-1}, shown in Figure 7, provide an explanation for the larger coupling contribution from the mode at 534 cm^{-1}. The 534 cm^{-1} vibration is mainly localized on the a-quinolate, whereas the 637 cm^{-1} vibration is delocalized, involving atomic displacement of the a-, b-, and c-quinolates.

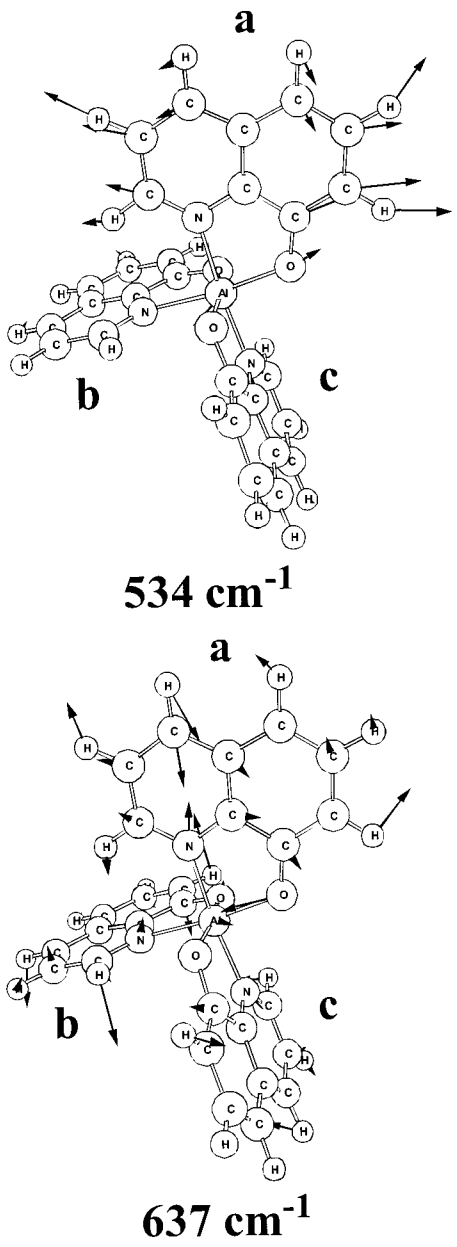

Figure 7. B-LYP/6-31G(d) normal mode atomic displacement vectors for vibrations at 534 and 637 cm^{-1}.

Conclusions

The first singlet excited state (S_1) of *mer*-Alq3 has been studied using the CIS/3-21+G** and TD-B3-LYP/

(53) In the theoretical prediction of molecular vibrational properties, density functional theory has been demonstrated to be a cost-effective alternative to conventional ab initio approaches, significantly outperforming Hartree−Fock while being of comparable computational cost. See: Scott, A. P.; Radom, L. *J. Phys. Chem.* **1996**, *100*, 16502. Wong, M. W. *Chem. Phys. Lett.* **1996**, *256*, 391. Halls, M. D.; Schlegel, H. B. *J. Chem. Phys.* **1998**, *109*, 10587. Halls, M. D.; Schlegel, H. B. *J. Chem. Phys.* **1999**, *111*, 8819.

3-21+G** levels of theory. The electronic excitation and the structural relaxation in the excited state for *mer*-Alq3 and for the free 8-hydroxyquinoline ligand have been interpreted in terms of the nature and nodal characteristics of the HOMO and LUMO. The correlation between the electronic excitation and the structural relaxation in the excited state for *mer*-Alq3 and for the free 8-hydroxyquinoline ligand has been made. The $S_0 \rightarrow S_1$ excitation is found to be mainly localized on the a-quinolate ligand as evidenced by the structural shift and the total electron density difference between the excited and ground electronic states of *mer*-Alq3. Through decomposition over ground-state normal modes, the coupling between the ground and excited state, through skeletal quinolate vibrations, occurs via the vibrational frequency at ca. 534 cm^{-1} in agreement with recent experimental studies, partly attributed to a high degree of localization on the a-quinolate. At the TD-B3-LYP level of theory, the calculated wavelength for emission and the Stokes shift agree very well with experiment.

Acknowledgment. Financial support from the National Science Foundation (Grant No. CHE9874005) and a grant for computing resources from NCSA (Grant No. CHE980042N) is gratefully acknowledged. M.D.H. thanks the Department of Chemistry, Wayne State University, for financial support provided by a Wilfred Heller Graduate Fellowship.

CM010121D